JOINT PHYSICAL OPTICS AND FDTD ANALYSIS OF MICROWAVE SCATTERING

B. Zhang[1], S. Primak,[1] J. LoVetri,[1] and S. Kashyap[2]

[1]Department of Electrical Engineering
The University of Western Ontario,
London, Ontario, Canada N6A 5B9
joe@gauss.engga.uwo.ca

[2]Department of National Defence
Defence Research Establishment Ottawa,
3701 Carling Ave., Ottawa, Ontario, Canada K1A 0K2

INTRODUCTION

The use of ultra-wideband radar for identification of targets has received considerable attention during the past two decades. In [1] a single target profile (*i.e.* the impulse response of a target taken at one aspect angle) was used to identify targets using the classical M-ary correlation receiver technique which was adapted to serve this purpose. However, it has been shown in [2] that even an optimal receiver produces poor results if an unknown signal is corrupted by noise. The performance of such a receiver also decays very fast with the number of possible targets [2]. As a consequence, multiple measurements must be performed. An alternative possibility is to build a synthetic aperture radar (SAR) image of the unknown target and to attempt to identify its major scattering centres, which are related to the geometry of the target [3-4]. Most of the models which have been used to build the SAR image of a target ignore the dispersive character of the scattering centres and any natural resonance of the target itself [5]. As a result, the image which is obtained is difficult to interpret and classify. Here we suggested a simple technique allowing one to obtain more tractable images by combining real measured data (or in our case, simulated data using FDTD) with those obtained from the Physical Optics (PO) approximation.

THE SIGNAL MODELS

The simplest radar model for a target is to model it as an ideal point scatterer of strength A located at position (x_0, y_0). Excited by a monochromatic electromagnetic plane-wave of frequency ω an ideal scatterer produces the normalized scattered field

Ultra-Wideband, Short-Pulse Electromagnetics 4
Edited by Heyman *et al.*, Kluwer Academic / Plenum Publishers, New York, 1999.

$$S(\omega, \varphi_i) = \frac{E^{sc}}{E^{inc}} e^{-2\boldsymbol{k}\cdot\boldsymbol{r}} = A\exp\left(-2j\frac{\omega}{c}x_0\cos\varphi_i - 2j\frac{\omega}{c}y_0\sin\varphi_i\right) \tag{1}$$

where $\boldsymbol{r}$ is the vector position of an *imaginary* centre of the target and $\boldsymbol{k}$ is the wave vector. Taking the 2-D inverse Fourier transform of (1) with respect to ω and observation angle φ_i (in the polar coordinate system), the following equation, giving rise to SAR imaging, can be obtained:

$$s(x, y) = A\delta(x - x_0)\delta(y - y_0). \tag{2}$$

In other words, ideal scattering centres correspond to ideal points in the SAR image [6]. Thus the reflectivity of the object in the $\omega - \varphi_i$ plane is simply the 2-D inverse Fourier transform of the scatterer geometry.

The later statement remains valid for a perfectly conducting body under the high frequency Physical Optics (PO) approximation [7]. For a perfectly conducting body illuminated by a plane monochromatic wave of wave number $\boldsymbol{k}$ and scatterers that are large compared to the wavelength of the excitation, the PO approximation states that the normalized monostatic response is given as [7]

$$\rho(\boldsymbol{k}) = \frac{S(\boldsymbol{k})}{I(\boldsymbol{k})} = \frac{j}{\sqrt{\pi}} \int_{\boldsymbol{k}\cdot\boldsymbol{n}<0} e^{-2j\boldsymbol{k}\cdot\boldsymbol{x}}\, \boldsymbol{k}\cdot d\boldsymbol{s}. \tag{3}$$

Here $I(\boldsymbol{k})$ is the incident plane wave, $S(\boldsymbol{k})$ is the scattered response, and $\boldsymbol{n}$ represents the outward normal to the surface of the scatterer and thus the condition $\boldsymbol{k}\cdot\boldsymbol{n} < 0$ represents the illuminated part of the body under consideration. If both $\boldsymbol{k}$ and $-\boldsymbol{k}$ are taken into account, the object is completely illuminated[1] and thus [8]

$$S(\omega, \varphi_i) = \rho(\boldsymbol{k}) + \rho^*(-\boldsymbol{k}) = \frac{2k^2}{\sqrt{\pi}} \int_V e^{-2j\boldsymbol{k}\cdot\boldsymbol{x}} dv. \tag{4}$$

In general, scattering from a real target cannot be approximated well by either an ideal point scatterer approximation, as in equation (1), or by the PO approximation, as given by equation (4). Two other physical phenomena, inherently present and not described by the PO approximation, are the frequency dependence of the scattering parameters and their dependence on the polarization of the incident wave. An advanced insight into these properties can be obtained in the context of the Geometrical Theory of Diffraction (GTD), valid under the assumption that the wavelength of the incident excitation is small relative to the targets extent [8]. It represents the normalized scattered field as originating from a set of M discrete scattering centres located at points (x_m, y_m), $1 \le m \le M$, *i.e.*

$$\rho(\omega, \varphi_i) = \sum_{m=1}^{M} S_m(\omega, \varphi_i)\exp\left[-2j\frac{\omega}{c_0}(x_m\cos\varphi_i + y_m\sin\varphi_i)\right], \tag{5}$$

where c_0 is the wave propagation velocity. The amplitude $S_m(\omega, \varphi_i)$ is a frequency and angle dependent coefficient, determined by the geometry, composition, and orientation of the corresponding scatterer. For the frequency dependence, GTD predicts [8] that the scattering amplitude is of the form $(j\omega)^{\alpha_m}$ where α_m is an integer multiple of $1/2$. Table 1 shows the relation between different values of the parameter α_m and the geometry of the scatterer [3]. The angle dependence of the magnitude of the scattered field is a much more complicated question. Most man-made targets, containing sharp edges can be characterized by a *sinc*-like aspect dependence of the scattering coefficient. In practice, especially, for the

1. The assumption that the target is a convex body is used at this step. However, a number of publications suggest that the results, obtained on the basis of equation (4) work well even if a target is not convex [9].

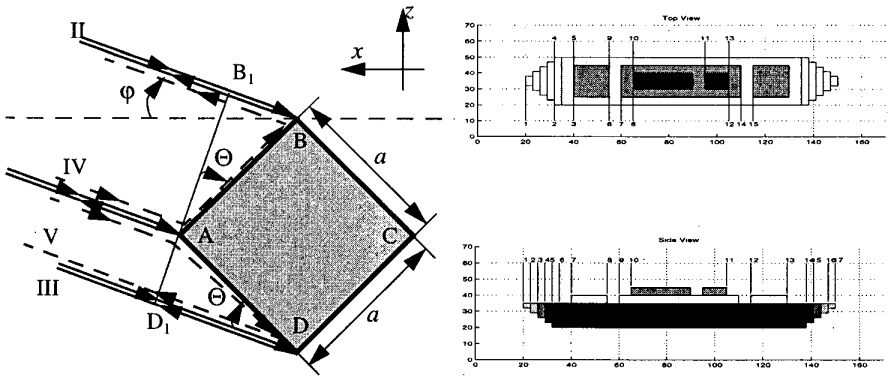

Figure 1. Geometry of the targets: a) rectangular plate, b) scaled ship model

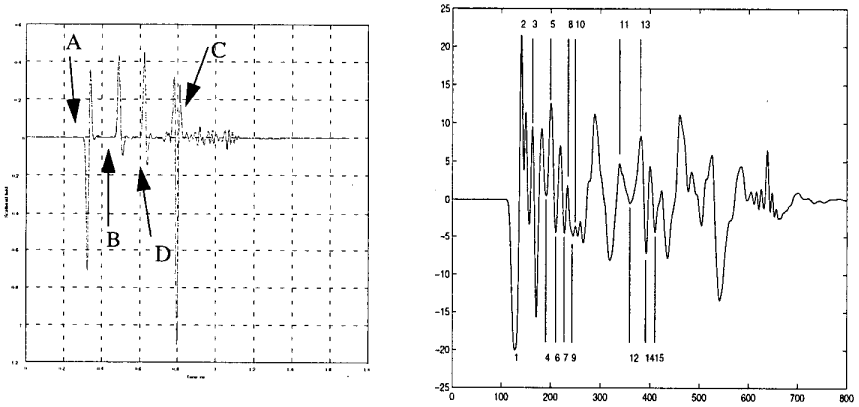

Figure 2. Scattering from a) rectangular plate, 30° aspect angle and b) simplified ship model, 30° aspect angle. Both calculated using FDTD.

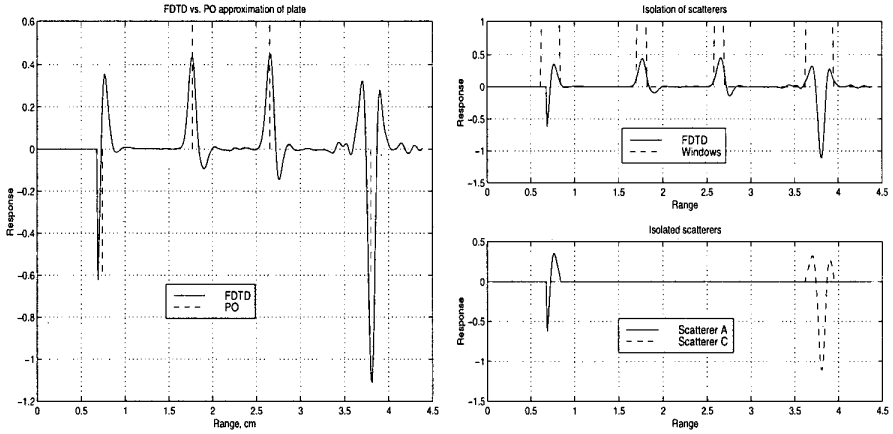

Figure 3. Sequential decomposition of FDTD response using PO approximation. The left picture shows "exact" FDTD response and locations and magnitudes of scattering centres estimated from the PO approximation. The top right figure shows the original signal with rectangular windows centred at the estimated scattering centres. The bottom right figure shows two isolated scattering centres, corresponding to $\alpha_1 = 2$ (edge A) and to $\alpha_4 = 4$ (edge C);

narrow-band of angles SAR, this dependence can be accurately approximated by an exponential, *i.e.* [3]

$$S(\omega, \varphi_i) = A_m(j\omega)^{\alpha_m} e^{\beta\varphi_i}. \tag{6}$$

The image of a target built on the basis of GTD is usually *different* from those obtained using the PO approximation. A single physical scatterer (for example plate corner) corresponds to three separate scatterers on the SAR image.

Table 1. Relation between parameter α and scatterer geometry

Value of α	Canonical scatterers
1	Flat plate at broadside; dihedral
1/2	Singly curved surface reflection
0	point scatterer; doubly curved surface reflection, straight edge specular
-1/2	curved edge diffraction
-1	corner diffraction

More problems can be encountered for relatively low frequencies (when the wavelength of the incident wave is larger then a target extent). The Singularity Expansion Method (SEM) [10] predicts that scattered waveforms can be represented as a sum of damped sinusoids in the time domain which results in "non-real" quasi-multiple scattering centres in the SAR image, which are not related to any real discontinuity in the target shape. This significantly complicates object identification.

JOINT PHYSICAL OPTICS - REAL DATA PROCESSING

Equation (4) can be simplified for the case of standard scatterers such as a rectangular plate. Consider a perfectly conducting plate of size $a \times b \times c$, then the scattering response derived from (4) can be simplified to

$$S(\omega, \varphi) = -\frac{16c}{\sqrt{\pi}} \frac{1}{\cos\varphi \sin\varphi} [e^{j(T_a+T_b)\omega} + e^{-j(T_a+T_b)\omega} - e^{j(T_a-T_b)\omega} - e^{-j(T_a-T_b)\omega}] \tag{7}$$

where c_0 is the speed of the wave and we have used the following notations

$$T_a = 2\frac{a\cos\varphi}{c_0}, \; T_b = 2\frac{b\sin\varphi}{c_0}. \tag{8}$$

Similar results can be obtained for a circular cylinder of radius R and length L

$$S(\omega) = \frac{2l\omega}{c_0\sqrt{\pi}} R J_1\left(\frac{2R\omega}{c_0}\right) \tag{9}$$

and a sphere of radius R

$$S(\omega) = -2\sqrt{\pi}R\cos\left(\frac{2R}{c_0}\omega\right) + \frac{c_0\sqrt{\pi}}{\omega}\sin\left(\frac{2R}{c_0}\omega\right). \tag{10}$$

It can be seen from (7-10) that this approximation properly predicts the locations of the scattering centres (for example at the edges of a plate and the centre of the sphere) and gives a good estimate for their magnitudes. At the same time it ignores the frequency dependence of the scatterer's response and the low-frequency portion of the response. It can be seen from equation (3) that the polarization of the scattered field yielded by the physical optics

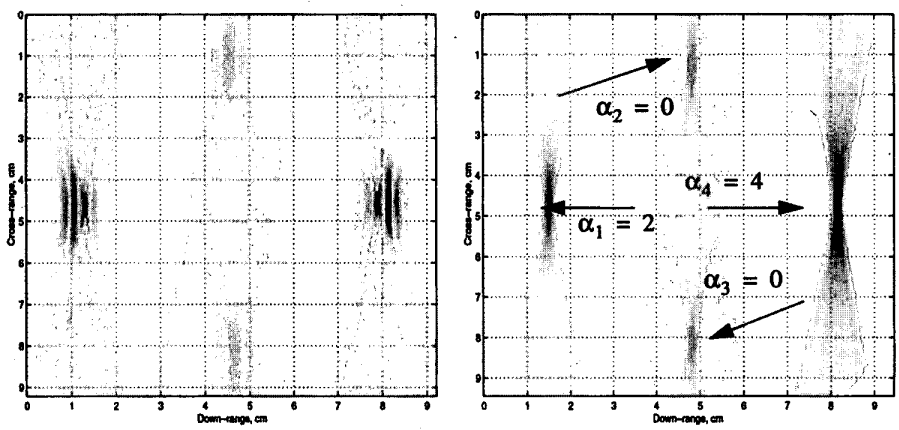

Figure 4. SAR image of the rectangular plate: a) obtained from the original FDTD data, b) obtained from PO approximation with GTD attributes attached.

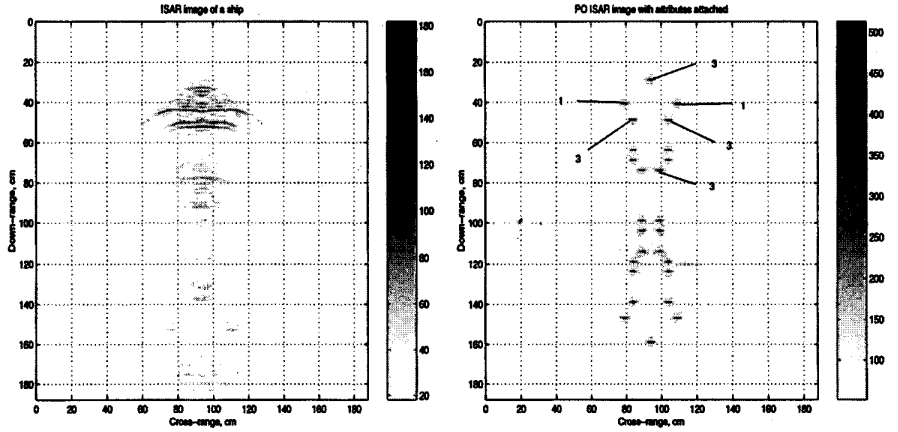

Figure 5. SAR image of a scaled model of a ship: a) obtained from the original FDTD data, b) obtained from PO approximation with GTD attributes attached.

approximation is co-linear with the incident field polarization. Thus, no polarization information can be obtained from the physical optics approximation.

Yet another important property of the PO approximation is the fact that if a body occupying volume V is subdivided into two, occupying volumes V_1 and V_2, such that the intersection of the two volumes is zero, *i.e.* $mes(V_1 \cap V_2) = 0$, according to (4), the normalized frequency response is just the sum of the frequency responses from each part V_1 and V_2 considered separately[1]. This gives us an opportunity to calculate the PO approximation for a complex object by dividing it into a set of simplified objects (for example in a set of rectangular, spheres or cylinders).

USING PO TO LOCATE SCATTERING CENTRES

Description of PO Based Technique

All the properties mentioned above, usually considered as a disadvantage of PO, can be used to obtain more tractable SAR images. As the first step, the main scattering centres are properly predicted by the PO approximation and extracted by any of the spectral estimation methods (Prony's, ESPRIT, Matrix Pencil, *etc.* [11]). The simple character of PO modelled scatterers (since PO does not model dispersive scatterers and resonances, see (7-10) for example) improves the performance of these spectral estimation methods which are known to be very sensitive to the number of poles to be extracted and their frequency dependence. In fact, a scatterer with $\alpha_m = 2$ and $\alpha_m = 3$ (points A and C in Fig. 2) can be considered as two or three closely located scatterers. At the same time there are two more simple scatterers (points B and D on the same figure). This fact leads to poor conditioned matrices used in estimation methods [11] which yields inaccurate results. This is not the case in PO approximation; thus the results are more numerically stable. The information extracted from PO data gives the position T_i and strength A_i of the i-th scatterer. A narrow time-domain window $w_{\alpha_m}(t, T_i)$ can be used to isolate a single scatterer.

$$r_w(t) = w_{\alpha_m}(t, T_i) r(t) \tag{11}$$

Here the window $w_{\alpha_m}(t, T_i)$ is assumed to be centred at $t = T_i$ and be $2\alpha_m$ times wider than the width of the excitation to obtain a more realistic response (FDTD, measurements, *etc.*). If α_m is not known *a priori*, the width of the window is iteratively increased until no changes in the estimated parameters are observed. Main steps of this technique are shown in Fig. 3. Using more realistic data allows to improve estimation of scatterer location and magnitude. SAR images obtained by joint PO and realistic data processing are closer to "optical" picture of a target than those obtained from raw realistic data (FDTD, measurements, *etc.*). However, they contain more information than those obtained just from PO.

The information extracted can also be used in identification of unknown targets. Classical approach, suggested in [10], requires estimation of scatterers locations directly from raw data with no *a priori* knowledge of their location nor of their dispersive nature. Such algorithms are very sensitive to noise, especially if the number of scatterers is not chosen properly. In addition, the dispersive nature of many man-made scatterers also causes difficulties in using such algorithms. Assuming that an unknown target is one of those included in a database one can try to estimate the corresponding scattering locations and the parameters α_m for each of them and compare the results to those stored in the database. It is

1. Once again a convexity of the target has to be assumed. However, if a target does not contain "strongly" non-convex parts, such as cavities, then convexity is not a very important assumption.

worthy to note that this can be done for multiple aspect measurements (since they all belong to the same target) and thus can be used to improve the performance of discrimination schemes. A similar situation exists if a SAR image is built from raw data. In many cases it can be overshadowed by resonances. If some assumptions are made about the target, a scatterer's location and strength can be estimated from the raw data, which will result in much cleaner SAR image. Let us emphasize again that if the right target is assumed, these estimates will be very consistent and will result in highly localized image. On the contrary if a wrong guess has been made the image which will be obtained will be very poor.

Examples: PEC Plate and Coarse Model of a Ship

The procedure suggested above was applied to the scattering response of a rectangular plate at the aspect angle $\varphi_i = 30^o$ (see Fig. 2). It can be seen from this figure that the scattering from the corners B and D look like simple reflections while the scattering from the corner A looks like the derivative of the incident pulse and the scattering from the corner C looks like the second derivative of the incident pulse. Application of Prony's method shows a different number of scattering centres which can be extracted from the windowed data. The corresponding results are shown in Table 2.

A number of SAR images, obtained using the FDTD code [12] and joint physical optics real data preprocessing are shown in Fig. 4-5. As was expected, this kind of preprocessing emphasizes the presence of the point scatterers at the corners of the plate and suppresses the oscillating nature of the scatterers. This can be clearly seen by comparing the corresponding pictures. At the same time, the ISAR image with preprocessing differs from those, obtained using physical optics approximation, involving real, unequal magnitude of the different scattering centres (see Table 2). This can be used in the identification problem, especially if some information about the properties of each scatterer is incorporated. For example, Moses [3] suggests to label each spot, corresponding to strong scatterers in accordance to Table 1. This is also shown in the Fig. 4-5 and gives more information about the object under investigation. Let us also note that the information contained in the low frequency (oscillatory) response can be ignored as the result of such preprocessing and "non-real" scattering centres can be avoided.

Table 2. Scattering centres information for a rectangular plate

Corner	Number of centres	Location, ns FDTD code	Predicted (PO) Location, ns	Normalized Amplitudes FDTD code
A	2	0.32, 0.34	0.33	0.65, -0.29
B	1	0.49	0.5	-0.32
C	3	0.78, 0.80, 0.82	0.81	-0.28, 1, -0.24
D	1	0.61	0.63	-0.34

CONCLUSIONS

A simple preprocessing algorithm of SAR data has been suggested. As the first step the information about the location of important non-dispersive scatterers predicted by the Physical Optics approximation is extracted and the corresponding SAR image is built. This image in many cases is similar to the "optical" image of the target and can be useful in target identification and training of human operators. As the next step more information can be

extracted from more accurate approximations of the real target response, such as the GTD approximation, FDTD or other numerical simulation. This additional information describes a shape of a specific scatterer predicted by PO. Extraction of the magnitude of the scatterers and their dispersive properties by conventional spectral estimation techniques can be simplified if time localization is used. The resonant behaviour of the target response can also be ignored which results in more clean and recognizable SAR images.

REFERENCES

1. H.J. Li and S.H. Yang, "Using Range Profiles as Feature Vectors to Identify Aerospace Objects," *IEEE Tran. Antennas and Propagation*, vol. 41, No.3, pp 582-588, March, 1993, pp. 261-268.
2. S. Primak, J. LoVetri, S. Kashyap, "A Comparative Study of UWB Radar Discrimination Schemes in a Noisy Background", presented on *1997 IEEE-AP International Symposium*, Montreal, Canada, July, 1997.
3. L. C. Porter, and R.Moses, "Attributed Scattering Centers for SAR ATR", *IEEE Transactions on Image Processing*, Vol. 6, No. 1, January, 1997, pp. 79-91.
4. C. Jakowatz, D. Wahl, P. Eichel, D. Ghiglia, and P. Thomson, *Spotlight-Mode Synthetic Aperture Radar: A Signal Processing Approach*, Kluwer, Boston, 1996.
5. S. Primak, J. LoVetri, Z. Damjanschitz, and S. Kashyap, "The E-pulse Technique for Dispersive Scatterers," in *Ultra-wideband, Short Pulse Electromagnetics* III, 1996, pp 327-334.
6. D.C. Munson, and R.L. Visentin, "A Signal processing View of Strip-Mapping Synthetic Aperture Radar", *IEEE Transaction on Acoustics, Speech and Signal Processing*, Vol. 37, No. 12, December, 1989, pp. 2131-2147.
7. N. Bojarski, "A Survey of the Physical Optics Inverse Scattering Identity", *IEEE Transactions on Antennas and Propagation*, Vol. AP-30, No. 5, September, 1982, pp. 980-989.
8. C. Balanis, *Advanced Engineering Electromagnetics*, John Wiley and Sons, New York, 1989.
9. E. Rothwell, K.M. Chen, D.P. Nyquist and J.E. Ross, "Time-Domain Imaging of Airborne Targets Using Ultra-Wideband or Short-Pulse Radar," *IEEE Transactions on Antennas and Propagation*, Vol. 43, No. 3, March 1995, pp.327-329.
10. C. Baum, E. Rothwell, K.-M. Chen, and D. Nyquist, "The Singularity Expansion Method and Its Applications to Target Identification", *Proc. IEEE*, Vol. 79, No. 10, October, 1991.
11. L. L. Sharf, *Statistical Signal Processing: Detection, Estimation, and Time Series Analysis*, Addison-Wesley, New York, 1991.
12. D. Mardare, J. LoVetri and R. Siushansian, *3-D EMFDTD User's Manual*, Developed at the Department of Electrical Engineering, Faculty of Engineering Science, The University of Western Ontario, 1996.